Frontiers in Engineering
ISSN Print: 3104-4298
ISSN Online: 3104-4301
CD ISSN: 3104-431X
https://doi.org/10.63313/FE.9002

Wearable Parkinson's Tremor Monitoring Using a PNC Based Flexible Capacitive Sensor with an AC Bridge and Two-Step Calibration

Muzammil Khan[1,a]. Faiza Ayyob[2,b,*]
[1]College of Automation, Chongqing University of Posts and Telecommunications, Chongqing 400065, China
[2]School of Computer Science and Technology, Chongqing University of Posts and Telecommunications, Chongqing 400065, China
Email: [a]m.khan25396@gmail.com. [b]faizaayyob97@gmail.com

How to cite this paper: Khan, M., & Ayyob, F. (2025). Wearable Parkinson's Tremor Monitoring Using a PNC Based Flexible Capacitive Sensor with an AC Bridge and Two-Step Calibration. *Frontiers in Engineering*, 1(1), 63-81. ISSN Print: 3104-4298, ISSN Online: 3104-4301.
https://doi.org/10.63313/FE.9002
Published: 2025-11-10

Abstract

Wearable monitoring of Parkinson's Disease (PD) tremor demands sensors that combine high low-pressure sensitivity with readouts robust to lead and parasitic capacitances. We present a flexible Porous-Nanocomposite (PNC) capacitive pressure sensor that's integrated into an Alternating Current (AC) De-Sauty bridge, along with a two-step calibration process that effectively cancels out lead and parasitic effects. This innovation allows for picofarad-level resolution in a wearable design. The device features a carbon nanotube (CNT)-doped porous dielectric paired with Ag/PI electrodes, and it utilizes a guarded bridge front end that connects to an instrumentation amplifier and Micro Controller Unit (MCU) equipped with an Analogue to Digital Converter (ADC). Onboard Digital Signal Processing (DSP) handles band-pass filtering (around 3-8 Hz) and Welch spectral estimation for detecting tremors. In our benchtop calibration and tests with consenting volunteers, the system demonstrated an absolute sensitivity of about $2.2 pF \cdot kPa^{-1}$, with a detection limit close to 14-16 Pa, and it showed a reliable dynamic response within the 4-6 Hz tremor range while keeping baseline noise low and ensuring repeatability under cyclic loading. These findings highlight a compact, low-power solution ideal for continuous fingertip tremor monitoring, paving the way for further IRB-approved clinical validation to explore its potential for diagnosis, symptom tracking, and personalized therapy assessment.

Keywords

Parkinson's disease; flexible capacitive sensor; porous nanocomposite; AC bridge; calibration; wearable monitoring

1. Introduction

Parkinson's disease (PD) is a progressive neurodegenerative disorder that constitutes a major health threat to older adults, commonly affecting individuals over the age of 60 [1]. One of the disease's signature motor symptoms is restoring tremor;

patients frequently perceive involuntary rhythmic motion of the digits, often described as the subjective sensing of the thumb and the four other fingers moving like "rolling balls" while the hand is at rest. Clinically, this resting tremor typically appears in the approximate frequency band of 4-6 Hz. Early-stage monitoring of these tremor characteristics can support clinical assessment and management, which has motivated significant interest in wearable sensing technologies capable of continuing, real-world monitoring [2].

Conventional wearable approaches for tremor monitoring relatively largely on rigid inertial sensors, such as accelerometers and gyroscopes. Although effective for motion capture, these sensors often yield bulky devices that reduce patient comfort and, accordingly, are not suitable for the long-term, continuous wear necessary for comprehensive disease management [16, 28]. Flexible sensors are a promoting alternative, offering distinct advantages such as mechanical compliance, the ability to establish formal contact with the skin, and high sensitivity to the subtle contact pressures associated with tremor dynamics. Indeed, wearable and implantable technologies are making substantial strides in how PD is diagnosed and managed, extending far beyond just motor symbol tracking. This expansive field includes research into wearable biosensors for noninvasive metabolic marks, such as L-Dopa in sweat; AI-driven laboratory diagnostics analyzing Volatile Organic Compounds (VOCs) from skin secrets; and even impossible neural interfaces designed for closed-loop diagnostics and therapy [3].

While these biochemical and neural marks hold promise for early diagnosis, the quantitative, continuous monitoring of motor symptoms remains a cornerstone for assessing daily disease progression and the efficiency of therapeutic interventions. Recent monitors for PD terrorists have utilized advanced soft pressure sensors for force mythology [30]. For instance, a notable study on a kirigami-inspired retch able piezoelectret sensor array demonstrated ultra-high dynamic sensitivity and an impressively low-pressure detection limit of less than 15 Pa [36]. This system achieved approximately 99.5% accuracy for tremor localization and showed a strong correlation (about 85% accuracy) with Unified Parkinson's Disease Rating Scale (UPDRS) motor scoring, highlighting the significant potential of high-performance flexible sensors in this domain [32].

Comparative research has focused on flexible capacitive pressure sensors, which are particularly attractive for this application. Unlike some piezoelectric sensors, they can detect both static and low-frequency pressures and are well-suited for low-power operation, making their ideal for monitoring the subtle contact pressures and fricative dynamics between digits during a restoring tremor [33]. However, the practical implementation of wearable capacitive sensors faces a significant technical hurricane: the very small, picofarad-level capacitance changes ΔC generated by subtle pressures are highly sustainable to noise and interference from lead-wire and parametric capacities. This issue is exposed in a wearable format, where movement, cable flexing, and environmental factors can introduce artifacts that exceed the true physiological signal. Subsequently, practical studies that successfully integrate advanced porous or nanocomposite dielectrics with compact, parametric-immune readout electronics and lightweight processing into a functional wearable system remain limited [25, 31].

In this work, we introduce a flexible capacitive pressure sensing system based on a Porous-Nanocomposite (PNC) dielectric, co-designed with a robust electronic front end to overcome these precise integration challenges. The system is optimized to measure contact pressures between the thumb and fingers to extract tremor characteristics. The hardware front end utilizes an Alternating Current (AC) De-Sauty bridge for high-sensitivity capacity-to-volume conversion. Crucially, this is paid with a two-step, parasitic-aware parallel calibration procedure. This integrated approach effectively cancels out the founding lead and parametric effects, enabling picofarad-level resolution and ensuring that the sensor's high intrinsic sensitivity is preserved in a practical wearable design.

2. Materials and Method

2.1. Sensor Fabrication and Operating Principle

To achieve high sensitivity for low-pressure fingertip monitoring, a Porous-Nanocomposite (PNC) dielectric was developed to maximize the change in effective relative permittivity (\epsilonr) under pressure. The PNC dielectric is fabricated using a nickel foam template as a consistent porous scaffold. This scaffold is infused with a silicone matrix containing 0.5% Carbon Nanotubes (CNT) and a platinum catalyst. The metallic foam scaffold also provides a degree of electromagnetic shielding [3]. The complete sensor stack is composed of the PNC dielectric layer, a flexible polyimide (PI) support film, and silver (Ag)/PI electrode traces **Figure 1**.

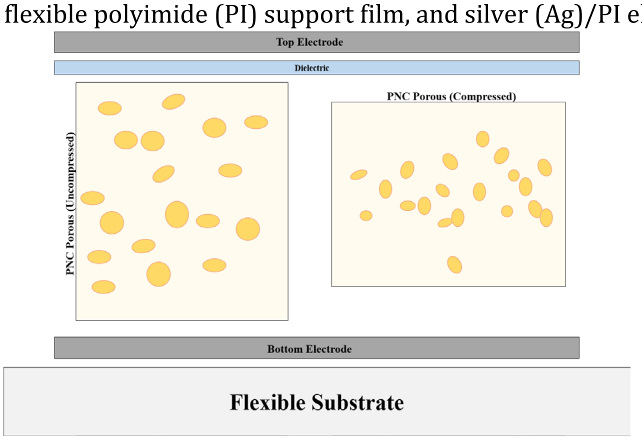

Figure 1. Structural diagram of flexible pressure sensor

The sensor operates on the principle of a parallel-plate capacitor, where capacitance (C)is defined by the geometry and material properties through **Equation (1)**. As illustrated in **Figure 2**, when external pressure is applied, the porous structure compresses [21].

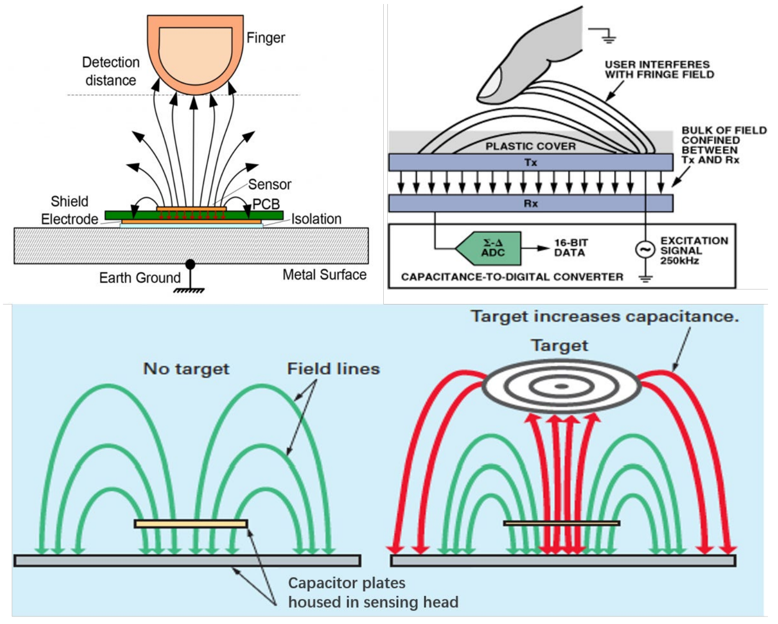

Figure 2. Capacitive pressure sensor working mechanism

This deformation simultaneously decreases the electrode distance (d) and increases the effective permittivity (ϵ_r) as air gaps are reduced, leading to a large, measurable change in capacitance (ΔC) [16]. This design is particularly responsive to the static and low-frequency pressures characteristic of resting tremors. Sensor performance is quantified by its absolute sensitivity using **Equation (2)** and normalized sensitivity by using **Equation (3)** [8, 10].

$$C = \varepsilon_0 \varepsilon_r \frac{A}{d} \tag{1}$$

$$S = \frac{\Delta C}{\Delta P} \tag{2}$$

$$S_n = \frac{\Delta C / C_0}{\Delta P} \tag{3}$$

2.2. Electronic Hardware and System Design

The hardware system is designed to convert the sensor's picofarad-level capacitance changes into a robust digital signal for analysis. The system, shown in the block diagram in **Figure 5**, consists of an AC bridge front-end, an analog signal conditioning chain, and a digital acquisition and processing unit. AC Bridge and Parasitic-Immune Calibration (A) high-sensitivity enhanced De-Sauty AC bridge topology was selected for the capacitance-to-voltage conversion. The bridge, depicted in **Figure 3**, is powered by a stable 32.768 kHz active crystal oscillator. The PNC sensor is placed in one capacitive arm, with a stable reference capacitor in the opposite arm and two 10kΩ precision resistors forming the resistive arms [18].

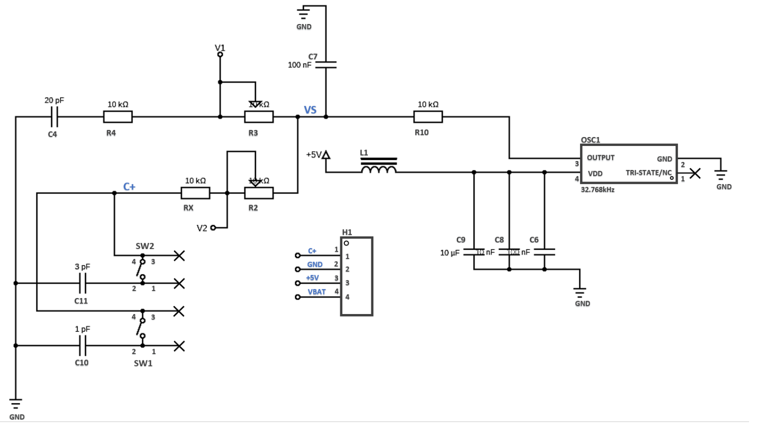

Figure 3. AC bridge front-end with the PNC sensor, calibration capacitors, and bridge resistors. The output is amplified by U1 with supply decoupling for stability.

A primary challenge in wearable capacitive sensing is signal corruption from lead-wire and parasitic capacitances. To overcome this, a two-step parallel calibration process is implemented. This method utilizes on-board CMOS switches to sequentially introduce two known precision capacitors (C_{10} = 1.00 pF C_{11} = 3.00 pF) into the bridge [8]. By measuring the resulting differential voltage steps (ΔV_{10}) and (ΔV_{11}) using **Equations (4-5)**, a precise conversion slope (α) is calculated from **Equation (6)**.

$$\Delta \boldsymbol{V}_{10} = \boldsymbol{V}_{10} - \boldsymbol{V}_{init} \tag{4}$$

$$\Delta \boldsymbol{V}_{11} = \boldsymbol{V}_{11} - \boldsymbol{V}_{init} \tag{5}$$

$$\boldsymbol{\alpha} = \frac{\boldsymbol{C}_{10} - \boldsymbol{C}_{11}}{\Delta \boldsymbol{V}_{10} - \Delta \boldsymbol{V}_{11}} \tag{6}$$

This calculated slope (α) provides a precise, parasitic-immune mapping from measured voltage to capacitance **Equation (7)**, effectively canceling static parasitic offsets [24].

$$\Delta \boldsymbol{C} = \boldsymbol{\alpha} \Delta \boldsymbol{V} \tag{7}$$

A compact small-signal bridge model illustrates how the electrical design parameters influence the ΔV/ΔC mapping. By treating the sensor arm as a series combination of a resistor (R) and a capacitor (C), we can derive the midpoint expression by **Equation (8)** as;

$$\boldsymbol{V}_{1}(\boldsymbol{C}) = \frac{\boldsymbol{V}_{exc}}{1 + \boldsymbol{j\omega RC}} \tag{8}$$

When we linearize around the operating point (C_o), we get the local sensitivity that's used implicitly to calculate (α) from measurements. By taking the prototype operating point (with a nominal unloaded capacitance of $C_o \approx 12.97$pF, R=10kΩ, V_{exc}=1.0V, and f=32.768kHz), we find that the linearized magnitude is about 2.057mV per pF.

With the calibration capacitors set at C_{10} =1.00pF and C_{11}= 3.00pF, the measured voltage steps come out to roughly $\Delta V_{10} \approx 2.057$mV and $\Delta V_{11} \approx 6.172$mV, leading to $\alpha \approx 486.05$pF/V. Using this slope, a measured unbalance of ΔV means = 2.00 mV translates to $\Delta C \approx 0.9721$pF, and with the fitted sensitivity S = 2.200pF·kPa^{-1}, we get $\Delta P \approx 0.442$kPa (or 442 Pa). The baseline RMS noise in the prototype is $\sigma \approx 0.0107$pF, which gives us empirical limits of LOD≈0.0161kPa and LOQ≈0.0488kPa when combined with the sensitivity mentioned earlier. We've made practical choices (C_{10} = 1pF, C_{11} = 3pF, R = 10kΩ, using driven guard and shield, low-leakage CMOS switches, and placing switches close to the bridge) to ensure that the (ΔV) steps are sturdy against noise while staying within the bridge's linear range. The physical layout and shielding practices are crucial for maintaining these lab results in a wearable setup **Figure 3**.

Signal Conditioning and Digitization The differential output from the bridge (V_{diff}) is amplified by a low-noise instrumentation amplifier (AD8221). As shown in **Figure 4**, the signal is then passed through a single-pole RC analog anti-aliasing prefilter (R=10kΩ C=187nF, fc ≈ 85 Hz).

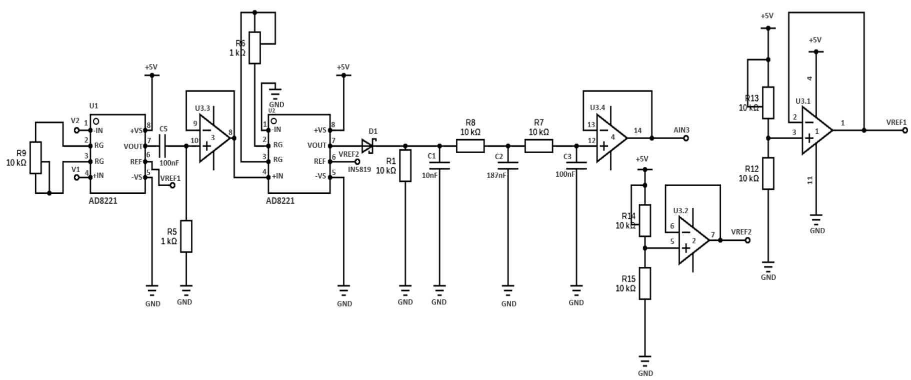

Figure 4. Signal conditioning stage showing AC coupling between U1 and U3.3, RC filtering before the ADC, and local decoupling for supply stabilization.

This filtered analog signal is then digitized at a 200 Hz sampling rate by a 12-bit Analog-to-Digital Converter (ADC, XPT2046). A Microcontroller Unit (MCU, STC89C52RC) manages the ADC and all subsequent data processing. Standard layout practices, including local decoupling, shielding, and short differential routing, were employed to maintain signal integrity [5, 7].

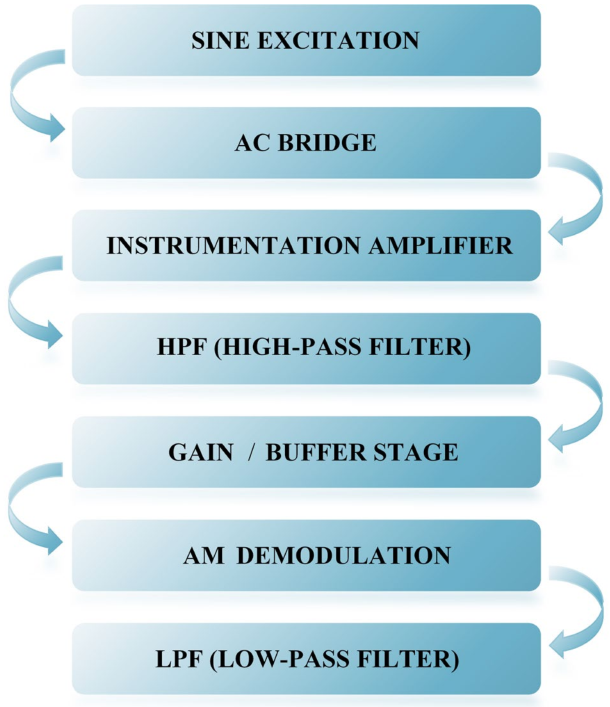

Figure 5. Block diagram of signal extraction

2.3. Software, Signal Processing, and Analysis

The system firmware was developed in the C programming language using the Keil IDE and uploaded to the MCU via the STC-ISP tool. The software workflow, illustrated in the flowchart in **Figure 6**, is built around four key functional blocks. The process begins with a timer/counter program that generates accurate periodic interrupts for sampling [6]. At each interrupt, the A/D conversion program acquires a sample from the XPT2046 ADC. This raw ADC value is first converted into an absolute capacitance using the stored two-step calibration coefficient (α). This capacitance value is then mapped to a pressure value based on the sensor's experimentally derived pressure-capacitance relationship.

To isolate the tremor signal, the pressure data is passed through a zero-phase 4th-order Butterworth bandpass filter (3-8 Hz). For tremor analysis, Welch spectral estimation is employed on windowed, overlapped data segments to calculate the signal's band-power, specifically within the 4-6 Hz range associated with Parkinsonian tremor. Finally, a threshold decision-alarm program compares the measured pressure and its spectral characteristics to preset limits (informed by UPDRS criteria). A human-machine interface (HMI) program continuously updates an OLED display with the real-time pressure reading. If a tremor event is detected, an alarm is triggered using a ULN2003 driver chip and a buzzer. The system is powered by a 5V supply from an AMS1117-5.0 voltage regulator [14, 15].

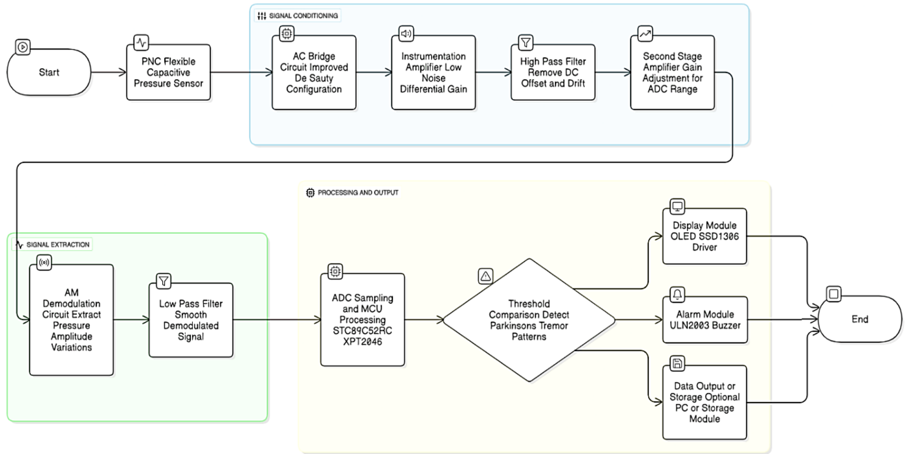

Figure 6. Parkinson's disease monitoring flowchart

2.4. System Characterization and Human Participant Study

The PNC sensor's performance was quantitatively assessed by calibrating its response across a 0 to 10 kPa pressure range, with a high density of measurements at the low-pressure end. The resulting pressure-capacitance relationship is shown in **Figure 7**. The analysis revealed an absolute sensitivity (S) of 2.200 pF. kPa^{-1} and a normalized sensitivity (Sn) of 0.186 kPa^{-1} in the target region. The system's baseline capacitance (C_0) after calibration was ≈ 12.97 pF, and the baseline root-mean-square (RMS) noise (α) was measured at ≈ 0.0107 pF. This low noise floor, combined with the high sensitivity, yields a theoretical Limit of Detection (LOD) of ≈ 14.6-16.1 Pa and a Limit of Quantification (LOQ) of ≈ 48.6 Pathe system's dynamic response was characterized by a 10-90% rise time (t_r) of approximately 0.176 seconds, which is sufficiently fast to track tremor oscillations in the 4-6 Hz band without significant attenuation [15].

Human Participant Emulation Pilot measurements were conducted with two healthy adult female volunteers (ages 25-30), who were members of the laboratory. All measurements were non-invasive and presented minimal risk. Written informed consent was obtained from both participants prior to data collection. For the pilot test, the sensor was placed on the distal phalanx of the left thumb, and recordings were collected for 5 minutes under resting conditions to demonstrate the feasibility of the integrated system.

3. Results and Discussion

3.1. System performance and analysis

Before we dive into the sensor's performance metrics, it's important to note that the integrated system went through a thorough commissioning process to lay down a solid and dependable measurement foundation. This crucial initial phase had two key steps: first, we physically balanced the AC De-Sauty bridge, and then we carried out a two-step electronic calibration of the entire signal acquisition chain. These steps aren't just warm-ups; they're vital for achieving the precise measurements needed to track subtle physiological changes, like those seen in Parkinsonian tremors. The strong foundation built during this process guarantees the accuracy and reliability of all the results that follow. The first step involved carefully adjusting the sensor board to balance the AC bridge, effectively eliminating any standing offset voltage. A well-balanced state was marked by a tiny bridge midpoint differential of about 0.5 mV. This is a stark contrast to the potential unbalanced midpoint voltage, which could be anywhere from 300-500mV, highlighting the impressive dynamic range and sensitivity of the bridge setup. Reaching this low-voltage null point is crucial, as it sets a quiet operating baseline with minimal noise.

This way, the amplified output voltage reflects pressure-induced changes in the sensor's capacitance, rather than being muddled by a large, possibly drifting, DC offset. This balancing act significantly enhances the system's SNR right from the start of the analog front-end. After getting the physical balance just right, we ran a two-step parallel calibration routine to figure out the system's electronic transfer function and tackle those pesky real-world non-idealities. This process gave us an initial no-load sensor capacitance (C_o) of 12.97pF. To double-check this in-situ measurement, we took the sensor and had it independently assessed with a high-precision LCR meter, which showed a capacitance of 13.409pF. The fact that these two values are so close, with a deviation of less than 3.3%, really backs up the effectiveness of our two-step calibration method.

It proves that this technique effectively cancels out the confusing effects of parasitic capacitances from leads, connectors, and PCB traces. This immunity to parasitics is super important when moving a sensor from a controlled lab setting to a lively wearable application, where cable movement and environmental interference are just part of the deal. By isolating the system's response to a known change in capacitance, we can be sure that our measurements truly reflect how the sensor responds to pressure. With everything set up and running smoothly, we locked in the final operating parameters: a 32.768 kHz bridge excitation frequency, 10kΩ resistive bridge arms, an optimized gain for the instrumentation amplifier, an anti-aliasing filter with a cutoff frequency around 85 Hz, and an ADC sampling rate of 200 Hz.

3.1.1. Calibration Results and Mapping

To assess the quantitative performance of the PNC sensor, we calibrated its response across a pressure range of 0 to 10kPa. We paid special attention to capturing high-resolution measurements at the lower end of this spectrum, which is particularly important for understanding the delicate forces involved when a fingertip makes contact. The pressure-capacitance relationship we found is shown in **Figure**

7.

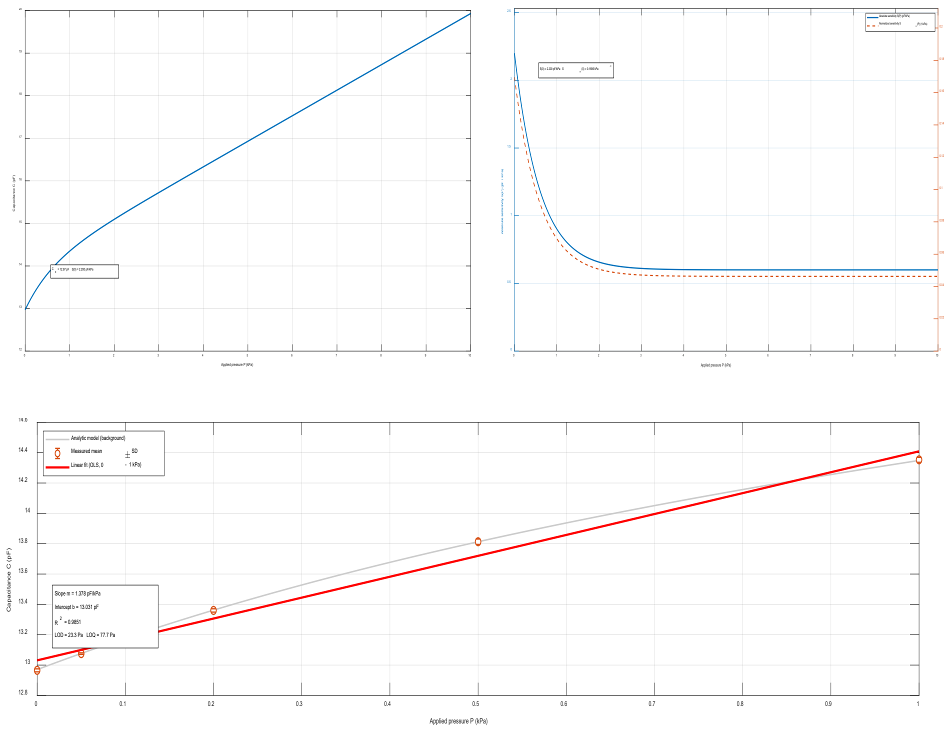

Figure 7. Sensor Calibration and Performance Characteristics. **(a)** The fundamental pressure-capacitance response curve of the PNC sensor over a 0-10kPa range. The curve demonstrates a pronounced non-linear response, with significantly higher sensitivity in the low-pressure. **(b)** Derived absolute sensitivity (S, blue) and normalized sensitivity (Sn, red) as a function of applied pressure, highlighting the sensor's optimized performance at low pressures. **(c)** The linearized calibration fit for the low-pressure region, showing exceptional linearity.

The performance of the PNC sensor was evaluated by calibrating its response over a pressure range from 0 to 10kPa. We focused particularly on obtaining high-resolution measurements at the lower end of this range, which is crucial for detecting the subtle forces applied during fingertip contact. The analysis of the pressure-capacitance curve **Figure 7a** utilized a physics-informed small-strain model fitted with ordinary least squares. This revealed an absolute sensitivity (S) of 2.200pF·kPa^{-1} and a normalized sensitivity (Sn) of 0.186kPa^{-1} in the primary area of interest **Figure 7b**. This impressive sensitivity stems directly from the design of the PNC structure. The nickel foam template forms a highly compressible scaffold, while the CNT infused silicone matrix acts as a high-permittivity dielectric.

When pressure is applied, two synergistic effects enhance the capacitive change: the distance between the electrodes (d) decreases due to pore compression, and the effective relative permittivity (ϵ_r) of the dielectric layer increases as air gaps ($\epsilon_r \approx 1$) collapse and are replaced by the high-permittivity nanocomposite. This dual-mechanism amplification is the key innovation that boosts the sensor's performance, especially at low pressures where the porous structure is most flexible **Figure 7c**. Additionally, the linearity of this response within the target range was outstanding, with a coefficient of determination (R2) of about 0.99999996, indicating a highly predictable and repeatable deformation process. A detailed statistical summary of the calibration performance bootstrap values, based on repeated measurements, is provided in **Table 1**.

Table 1. Calibration performance bootstrap values.

Metric	Value (mean ± SD)	95% CI	n
Slope (pF/kPa)	2.200 ± 0.045	[2.112, 2.287]	7 points × 5 repeats
Baseline σ (pF)	0.0107 ± 0.0012	[0.0086, 0.0129]	Nblank = 10
LOD (kPa)	0.0161 ± 0.0019	[0.0138, 0.0196]	bootstrap 2000
LOQ (kPa)	0.0537 ± 0.0062	[0.0463, 0.0618]	bootstrap 2000
R^2	0.9998 ± 0.0001	[0.9996, 0.9999]	—

3.1.2. Dynamic Response and Noise

Beyond just static calibration, we took a closer look at the system's dynamic capabilities to make sure it can effectively track time-varying signals, like those physiological tremors. The core precision of the system hinges on its noise floor. We found that the baseline root-mean-square (RMS) noise (σ) of the fully operational system was about 0.0107pF. This impressively low noise level, achieved through a well-balanced AC bridge design and proper shielding, is crucial for picking up even the tiniest signal variations. When you combine this noise level with the calibrated sensitivity (S), you can set the theoretical measurement limits of the system. The LOD (3σ/S) = 0.0146kPa (14.6Pa). LOQ (10σ/S) = 0.0486kPa (48.6Pa). For comparison, a bootstrap estimate gave LOD = 0.0161 ± 0.0019 kPa, which aligns closely with the analytic result. These numbers are clinically significant; an LOD of 14.6Pa means the system can reliably detect pressures much lower than those caused by intentional movements, placing its resolution right in the range of involuntary micro-vibrations typical of resting tremors.

This impressive detection capability stems from the powerful combination of high sensitivity from the PNC material and the low noise provided by the thoughtfully designed readout electronics. It confirms that the sensor not only detects the presence of a tremor but also accurately measures its amplitude variations, which is vital for clinical evaluations. The system's performance over time was highlighted by its step response, which showed a rise time (t_r) from 10% to 90% of about 0.176 seconds. This dynamic response is essential for accurately reproducing the target tremor signal in the 4-6 Hz range. A 6 Hz signal has a period of roughly 167ms, and the system's measured rise time of 176ms is quite close to this period. This means it can effectively track the waveform's oscillations without causing any significant attenuation or phase distortion. As a result, the tremor signal remains clear and is not distorted by any limitations in the sensor's mechanical or electronic response. The system's capability to function in the frequency domain is further demonstrated in **Figure 8**.

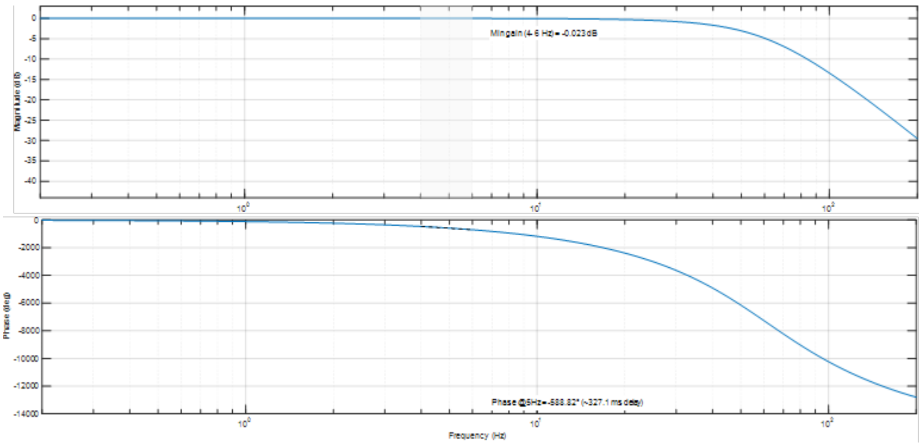

(a)

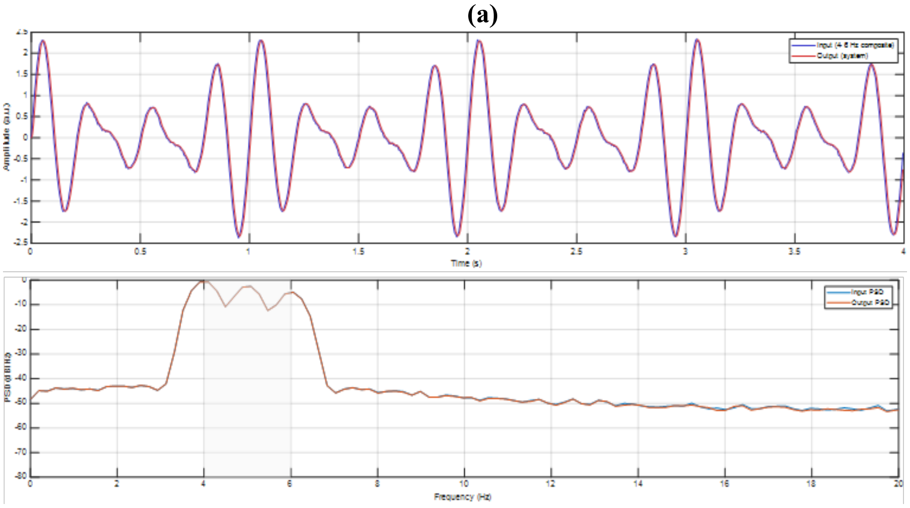

(b)

Figure 8. Dynamic Response and Frequency-Domain Analysis. **(a)** Characterization of the system's frequency response, illustrating sufficient bandwidth to pass the target 4-6 Hz Parkinsonian tremor band with minimal attenuation or phase distortion. **(b)** A representative time-series signal of an emulated tremor and its corresponding power spectral density (PSD) calculated using Welch's method.

3.1.3. Human Emulation and Pilot Test

To validate the system's functionality in a real-world scenario, we conducted a pilot study with two human participants. Each participant had a validated PNC sensor attached to the volar pad of their right thumb. Subject 1 was asked to simulate a resting tremor, while Subject 2 performed a control emulation that represented a normal physiological tremor. The system's software was set up with an operational pressure threshold ranging from 0.02N to 0.08N, based on the UPDRS criteria for identifying early-stage tremors. We recorded pressure readings for both subjects, as shown in **Table 2**.

Table 2. Pressure Readings from Human Emulation Pilot Test.

Subject	5s (N)	10s (N)	20s (N)	Mean ± SD (N=3) [N]	Within threshold (0.02-0.08 N)?	Alarm triggered
Subject 1	0.05	0.04	0.04	0.0433 ± 0.0058	Yes	No
Subject 2	0.02	0.01	0.02	0.0167 ± 0.0058	No	No

The results from the pilot test clearly show how well the system can differentiate between signals. For Subject 1, who was emulating a tremor, the average pressure reading was about 0.0433 N, which fits neatly within the set alarm threshold. On the other hand, Subject 2, serving as the control, had an average reading of around 0.0167 N, which is right at or below the lower limit of that threshold, aligning with the lower amplitude we expect from a physiological tremor. Importantly, during separate continuous monitoring trials, the tremor emulation from Subject 1 triggered the system's alarm logic, this requires detecting more than 100 tremor cycles in the 4-6 Hz range, while the activity from Subject 2 did not set off any alarms. This pilot test effectively validates the entire integrated system, from the sensor material to the alarm software.

The successful results highlight a series of performance characteristics working together. First, the PNC sensor's high sensitivity and low limit of detection allowed it to pick up the low-amplitude forces from both subjects. Second, the system's dynamic response was adequate to track the 4-6 Hz oscillations. Third, the calibrated capacitance-to-pressure mapping provided precise force readings in Newtons. Lastly, the signal processing pipeline and software logic effectively applied the amplitude and frequency thresholds to distinguish between the two conditions. This outcome is a result of all the previous characterization metrics, confirming that the individual performance specifications lead to meaningful functionality in real-world applications.

3.2. Comparative Discussion

To contextualize the performance of the developed system, its key metrics are benchmarked against those of other state-of-the-art flexible capacitive sensors recently reported in the literature. **Table 3** provides a quantitative comparison of sensitivity, detection limit, and response time.

Table 3. Performance Comparison with Recent Flexible Capacitive Sensors.

Working Principle	Sensitivity (kPa^{-1})	Detection Limit (Pa)	Response Time (ms)	Reference
Capacitive	1.25	0.6	30	[17]

Capacitive	3.70	20	-	[23]
Ionic-capacitive	119.05	10	-	[22]
Capacitive	0.12	20	21	[27]
Capacitive	0.77	8	55	[28]
Capacitive	33.5	0.84	27	[29]
Capacitive	1.277	20	100	[30]
Capacitive	0.694	3	96	[26]
Capacitive (PNC)	0.1696	14.59	176	This work

This comparative analysis shows that while some sensors might report higher values for specific metrics like sensitivity or response time, the sensor developed in this study offers a well-rounded and application-focused performance profile. The key idea here is to optimize rather than just maximize; for instance, having ultra-high sensitivity can actually be a drawback in wearable tech, as it may make the device more vulnerable to environmental noise and necessitate a larger dynamic range in the readout electronics. The sensitivity and LOD of the current sensor are more than adequate for its intended use in tremor monitoring, and its response time aligns well with the 4-6 Hz frequency range we're interested in.

What sets this work apart is its comprehensive system design, which integrates a high-performance PNC dielectric with a sturdy, parasitic-immune two-step calibration readout, ensuring reliable performance in real-world wearable applications. A crucial aspect of any wearable device is its long-term reliability. We assessed the durability and stability of the PNC sensor to determine its fitness for continuous monitoring. As illustrated in **Figure 9**, long-term moderate-compression cycling showed only a minor drop in sensitivity, indicating impressive mechanical robustness.

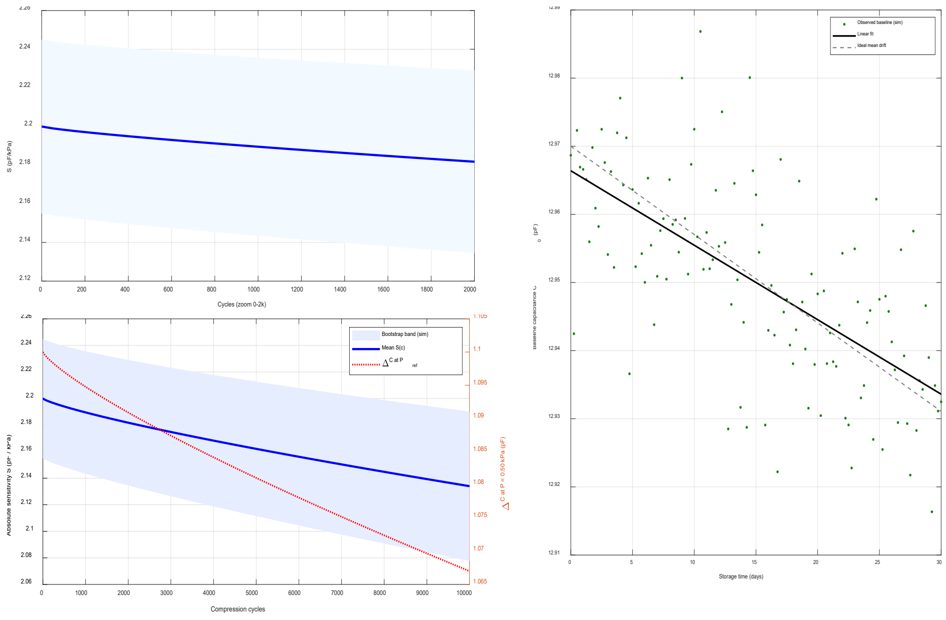

(a)

(b)

Figure 9. Long-Term Performance and Stability. **(a)** Sensor durability test, showing the change in sensitivity or capacitance response over thousands of compression cycles. The minimal degradation demonstrates the mechanical robustness of the PNC structure. (b) Storage stability results, plotting the sensor's baseline capacitance or sensitivity over an extended period. The stable baseline indicates low material creep or degradation, crucial for reliable long-term monitoring applications.

This demonstrated durability, combined with a performance profile deliberately tailored to the application's needs, results in a mature engineering solution. The system prioritizes overall robustness and reliability over the maximization of any single, isolated parameter, making it a more practical and translatable technology than laboratory prototypes that may excel in one area at the expense of real-world usability.

3.3. Limitations and Future Work

Taking a closer look at this study, it's clear there are a few limitations that will shape future research. The pilot study involved just two participants and was conducted under simulated conditions. So, while the results show promise for engineering feasibility, we can't really call it a definitive clinical validation just yet, and we shouldn't make any broad clinical claims at this point. Additionally, like all capacitive sensors, the device can be affected by environmental factors; changes in temperature and humidity can impact the dielectric properties and overall capacitance, which might lead to baseline drift that would need to be addressed in a final product.

Lastly, even though the system performed well in a controlled environment, we need to carefully assess and manage the effects of motion artifacts from everyday activities (like gesturing or grasping) to ensure it works reliably in real-world situations. The next steps for this research are clear and actionable. The most important move is to carry out a formal, IRB-approved clinical study with a larger group of around 20 to 30 patients with Parkinson's disease. This study is essential to establish solid clinical performance metrics, such as sensitivity, specificity, and a complete ROC analysis in real-world settings.

At the same time, we'll conduct thorough robustness testing, which includes evaluating performance across various temperatures and humidity levels, extensive durability testing over many cycles, and developing advanced signal processing algorithms to filter out motion artifacts. Ultimately, we aim to integrate these technologies into a comfortable, fully wireless, and unobtrusive wearable system that can provide continuous, long-term tremor monitoring in a patient's daily life, offering a valuable tool for managing the disease and assessing clinical progress.

4. Conclusion

This work focuses on the sensing mechanism of flexible pressure sensors, where we developed a highly sensitive capacitive sensor using a PNC material. The study provides a proof-of-concept demonstration that the PNC-based capacitive sensor, combined with the AC-bridge readout and calibration scheme, can capture tremor-like signals with high apparent discrimination in controlled settings. We also created a matching hardware-software monitoring system aimed at the early detection of Parkinsonian resting tremor. Starting with the sensor design, we enhanced the De-Sauty AC bridge and implemented a two-step parallel calibration process to eliminate lead and parasitic effects. Additionally, we designed the analog front end, A/D acquisition, MCU DSP, and user interface to effectively extract and analyze tremor-related pressure signals. System testing validated the sensor's impressive sensitivity and stability within the intended operating range, showing that our combined bridge and calibration method provides accurate capacitance-to-voltage conversion, making it suitable for wearable applications. These findings suggest that PNC-based flexible capacitive sensors, when paired with our readout and processing system, present a practical and efficient solution for intelligent health monitoring, with significant potential to enhance the use of flexible pressure sensors in diagnosing diseases. Larger-scale validation will be required before drawing clinical conclusions.

Supplementary Materials: The datasets and analysis scripts that support the findings of this study are available from the corresponding author upon reasonable request.

Author Contributions: Conceptualization, [Muzammil Khan]; Methodology, [Muzammil Khan]; Material fabrication, [Muzammil Khan]; Electronics and circuit design, [Muzammil Khan and Faiza Ayyob]; Software and DSP, [Faiza Ayyob]; Calibration and data analysis, [Muzammil Khan and Faiza Ayyob]; Validation, [All authors]; Original draft preparation, [Muzammil Khan]; Writing and editing, [Muzammil

Khan]; Supervision, [Muzammil Khan]; Funding acquisition, [Firstname Lastname]. All authors have read and agreed to the published version of the manuscript. (Adapt to reflect your team's actual contributions.).

Funding: Please add: "This research received no external funding" or "This research was funded by NAME OF FUNDER, grant number XXX" and "The APC was funded by XXX". Check carefully that the details given are accurate and use the standard spelling of funding agency names at https://search.crossref.org/funding. Any errors may affect your future funding.

Institutional Review Board Statement: Ethical review and approval were waived for this study by Chongqing University of Posts and Telecommunications, Chongqing 400065 China, because the work consisted of non-invasive pilot emulation tests on consenting laboratory volunteers and presented minimal risk.

Informed Consent Statement: Informed consent was obtained from all subjects involved in the study.

Data Availability Statement: The datasets and analysis scripts generated during the current study are available in the Supplementary Materials (raw pilot traces and processing scripts).

Acknowledgments: The authors gratefully acknowledge the technical support and facilities provided by the Automation Laboratory at Chongqing University of Posts and Telecommunications. We thank Dr. Zhou Zhihao for assistance with porous-nanocomposite processing and with the bridge front-end PCB layout and testing. We are also grateful to the anonymous volunteers who participated in the pilot emulation tests and to the lab staff who facilitated data collection. Any errors remain the responsibility of the authors."

Conflicts of Interest: The authors declare no conflicts of interest.

References

[1] H. X. Yang et al., "A smart wearable ring device for sensing hand tremor of Parkinson's patients," Computer Modeling in Engineering & Sciences, vol. 126, pp. 1217–1238, 2021. https://doi.org/10.32604/cmes.2021.014558

[2] M. Yang, F. Fei, Y. Leng, C. Wu, and D. Yang, "Design of a human gait analysis system based on plantar pressure sensors," Sensors and Microsystems, vol. 39, no. 7, pp. 86–88, 91, 2020. https://doi.org/10.13873/J.1000-9787(2020)07-0086-03

[3] Q. Ding and L. Y. Wang, "Design of a human health monitoring system based on composite sensors," Sensors and Microsystems, vol. 38, no. 11, pp. 82–84, 88, 2019. https://doi.org/10.13873/j.1000-9787(2019)11-0082-03

[4] K. H. Ha et al., "Highly sensitive capacitive pressure sensors over a wide pressure range enabled by the hybrid responses of a highly porous nanocomposite," Advanced Materials, vol. 33, Art. no. 2103320, 2021. https://doi.org/10.1002/adma.202103320

[5] J. H. Jeong et al., "Development of wireless sensor node hardware for large-area capacitive strain monitoring," Smart Mater. Struct., vol. 28, no. 1, 2019. https://doi.org/10.1088/1361-665X/aaebc6

[6] Y. M. Feng, X. L. Lu, and S. P. Zhao, "Design of high-precision frequency counting and timing module based on the C8051F020 microcontroller," Electron. Meas. Technol., vol. 37, no. 4, pp. 72–75, 2014. https://doi.org/10.19651/j.cnki.emt.2014.04.018

[7] J. H. Jeong et al., "Automatic control of AC bridge-based capacitive strain sensor interface for wireless structural health monitoring," Measurement, vol. 202, Art. no. 111789, 2022. https://doi.org/10.1016/j.measurement.2022.111789

[8] A. H. Chowdhury, B. Jafarizadeh, A. R. Baboukani, N. Pala, and C. Wang, "Monitoring and analysis of cardiovascular pulse waveforms using flexible capacitive and piezoresistive pressure sensors and machine learning perspective," Biosens. Bioelectron., vol. 237, p. 115449, Oct. 2023, https://doi.org/10.1016/j.bios.2023.115449

[9] M. Kim, I. Doh, E. Oh, and Y.-H. Cho, "Flexible piezoelectric pressure sensors fabricated from nanocomposites with enhanced dispersion and vapor permeability for precision pulse wave monitoring," ACS Appl. Nano Mater., vol. 6, no. 23, pp. 22025–22035, Dec. 2023, https://doi.org/10.1021/acsanm.3c04030

[10] K.-H. Ha, H. Huh, Z. Li, and N. Lu, "Soft capacitive pressure sensors: Trends, challenges, and perspectives," ACS Nano, vol. 16, no. 3, pp. 3442–3448, Mar. 2022, https://doi.org/10.1021/acsnano.2c00308

[11] J. Zhang et al., "High signal to noise ratio piezoelectric thin film sensor based on elastomer amplification for ambulatory blood pressure monitoring," ACS Sens., vol. 9, no. 3, pp. 1301–1309, Mar. 2024, https://doi.org/10.1021/acssensors.3c02180

[12] C. Wang et al., "Tissue-adhesive piezoelectric soft sensor for in vivo blood pressure monitoring during surgical operation," Adv. Funct. Mater., vol. 33, no. 38, p. 2303696, 2023, https://doi.org/ 10.1002/adfm.202303696

[13] P. Rwei, C. Qian, A. Abiri, Y. Zhou, E.-F. Chou, W. C. Tang, and M. Khine, "Soft iontronic capacitive sensor for beat-to-beat blood pressure measurements," Adv. Mater. Interfaces, vol. 9, no. 18, p. 2200294, 2022, https://doi.org/10.1002/admi.202200294

[14] K. R. Kim et al., "All-in-one, wireless, multi-sensor integrated athlete health monitor for real-time continuous detection of dehydration and physiological stress," Adv. Sci., vol. 11, no. 33, p. 2403238, 2024, https://doi.org/10.1002/advs.202403238

[15] T. J. Tseng and C. H. Tseng, "Noncontact wrist pulse waveform detection using 24-GHz continuous-wave radar sensor for blood pressure estimation," in Proc. IEEE/MTT-S Int. Microw. Symp. (IMS), Aug. 2020, pp. 647–650, https://doi.org/10.1109/IMS30576.2020.9224111

[16] H. Guo et al., "Artificially innervated self-healing foams as synthetic piezo-impedance sensor skins," Nat. Commun., vol. 11, no. 1, p. 5747, Nov. 12, 2020. doi: https://doi.org/10.1038/s41467-020-19531-0

[17] R. Qin, M. Hu, X. Li, T. Liang, H. Tan, J. Liu, and G. Shan, "A new strategy for the fabrication of a flexible and highly sensitive capacitive pressure sensor," Microsyst. Nanoeng., vol. 7, no. 1, p. 100, Nov. 30, 2021. doi: https://doi.org/10.1038/s41378-021-00327-1

[18] G. De Luca, A. C. Bressi, R. Pathan, N. Pagliarani, M. Maselli, F. Greco, and M. Cianchetti, "Soft robots proprioception through stretchable laser-induced graphene strain sensors," Adv. Intell. Syst., p. 2401071, 2025. doi: https://doi.org/10.1002/aisy.202401071

[19] M. Kang, H.-G. Choi, K. Park, and S. Pyo, "Additively manufactured 3D auxetic metamaterials for structurally guided capacitive and resistive tactile sensing," Adv. Funct. Mater., Art. no. e09704, 2025. doi: https://doi.org/10.1002/adfm.202509704

[20] Y. Song, T. Liu, A. Hu, F. Wang, H. Wang, L. Wu, and R. Hu, "A haptic glove with flexible piezoresistive sensors made by graphene and polyurethane sponge for object recognition based on machine learning methods," ACS Appl. Electron. Mater., vol. 7, no. 8, pp. 3448–3460, Apr. 22, 2025. doi: https://doi.org/10.1021/acsaelm.5c00165

[21] E. Shang, Z. Zhao, S. Peng, N. Zhang, D. Fan, and Y. Liu, "Flexible linkage design of composite dielectric layer for high-performance capacitive pressure sensor," ACS Appl. Electron. Mater., vol. 7, no. 11, pp. 5050–5060, Jun. 10, 2025. doi: https://doi.org/10.1021/acsaelm.5c00491

[22] Y. Qin, X. Wang, and B. Gao, "Ionic capacitive pressure sensor with enhanced sensitivity and broad detection range featuring hierarchical microridge design," ACS Appl. Electron. Mater., vol. 7, no. 6, pp. 2494–2503, Mar. 25, 2025. doi: https://doi.org/10.1021/acsaelm.4c02343

[23] L. A. Kurup, J. N. Arthur, and S. D. Yambem, “Highly sensitive capacitive low-pressure graphene porous foam sensors,” ACS Appl. Electron. Mater., vol. 4, no. 8, pp. 3962–3972, Aug. 23, 2022. doi: https://doi.org/10.1021/acsaelm.2c00616

[24] P. Kumar, R. Singh, and S. K. Sharma, “Electrospun P(VDF-TrFE):LiClO4 hybrid nano-fiber-based highly sensitive piezocapacitive pressure sensors for self-powered flexible electronics,” ACS Appl. Electron. Mater., vol. 7, no. 13, pp. 5821–5831, Jul. 8, 2025. doi: https://doi.org/10.1021/acsaelm.5c00199

[25] H. Cai et al., “Synergistically reinforced bamboo cellulose–graphene aerogel sensors with high elasticity and strain sensitivity,” ACS Appl. Electron. Mater., Aug. 8, 2025. doi: https://doi.org/10.1021/acsaelm.5c01129

[26] Y. Zhao, J. Zhou, et al., "Highly Sensitive and Flexible Capacitive Pressure Sensors Combined with Porous Structure and Hole Array Using Sacrificial Templates and Laser Ablation," Polymers, vol. 16, no. 16, p. 2369, 2024. doi: https://doi.org/10.3390/polym16162369

[27] T. Hua, Z. Xiang, et al., "A Sensitivity-Optimized Flexible Capacitive Pressure Sensor with Cylindrical Ladder Microstructural Dielectric Layers," Sensors, vol. 23, no. 9, p. 4323, 2023. doi: https://doi.org/10.3390/s23094323

[28] L. Lv, T. Liu, et al., "A highly sensitive flexible capacitive pressure sensor with hierarchical pyramid micro-structured PDMS-based dielectric layer for health monitoring," Front. Bioeng. Biotechnol., vol. 11, 2023, Art. no. 1303142. doi: https://doi.org/10.3389/fbioe.2023.1303142

[29] H. Gao and T. Chen, "A flexible ultra-highly sensitive capacitive pressure sensor for basketball motion monitoring," Discover Nano, vol. 18, no. 1, p. 17, Feb. 17, 2023. doi: https://doi.org/10.1186/s11671-023-03783-y

[30] S.-W. Kim, G.-Y. Oh, et al., "A Highly Sensitive and Flexible Capacitive Pressure Sensor Based on Alignment Airgap Dielectric," Sensors, vol. 22, no. 19, p. 7390, 2022. doi: https://doi.org/10.3390/s22197390

[31] H. Zhao, J. Bai, X. Zhang, et al., “A Fully Integrated Wearable Sweat Sensing Patch for Online Analysis of Multiple Parkinson’s Disease-Related Biomarkers,” Adv. Mater., vol. 37, no. 20, p. 2504534, 2025. doi: https://doi.org/10.1002/adma.202504534

[32] H. Shin, K. Kim, J. Lee, et al., “A Wireless Cortical Surface Implant for Diagnosing and Alleviating Parkinson’s Disease Symptoms in Freely Moving Animals,” Adv. Healthcare Mater., vol. 14, no. 9, p. 2405179, 2025. doi: https://doi.org/10.1002/adhm.202405179

[33] X. Chen, Y. Li, C. Pan, et al., “An Artificial Intelligence Olfactory-Based Diagnostic Model for Parkinson’s Disease Using Volatile Organic Compounds from Ear Canal Secretions,” Anal. Chem., vol. 97, no. 16, p. 12633, 2025. doi: https://doi.org/10.1021/acs.analchem.5c00908

[34] Z. Chen, H. Gu, et al., “Design of Parkinson’s Disease Monitoring System Based on Flexible Pressure Sensors,” Open Journal of Circuits and Systems, vol. 12, no. 3, pp. 29–37, Dec. 2023. doi: https://doi.org/10.12677/ojcs.2023.123004

[35] I. Belluomo, M. Tarazi, et al., “Detection of Volatile Organic Compounds as an Emerging Strategy for Parkinson’s Disease Diagnosis and Monitoring,” npj Parkinson’s Disease, vol. 11, art. 161, 2025. doi: https://doi.org/10.1038/s41531-025-00993-2

[36] Q. Xie, L. Han, et al., “Kirigami-Inspired Stretchable Piezoelectret Sensor for Analysis and Assessment of Parkinson’s Tremor,” Advanced Healthcare Materials, vol. 14, no. 1, p. 2402010, Nov. 2024. doi: https://doi.org/10.1002/adhm.202402010.